J. Fluid Mech. (2002), *vol.* 473, *pp.* 321–347.
DOI: 10.1017/S0022112002002483 Printed in the United Kingdom

On the capillary interaction between solid plates forming menisci on the surface of a liquid

By TAHER A. SAIF

Department of Mechanical and Industrial Engineering, University of Illinois,
1206 West Green Street, Urbana, IL 61801, USA

(Received 22 March 2001 and in revised form 10 July 2002)

A hydrophilic or a hydrophobic long rigid solid plate of finite width, forming a meniscus with a liquid in a uniform gravitational field is considered. The one-dimensional meniscus with prescribed heights of the triple point from the far-field liquid surface is investigated analytically using the Young–Laplace equation. It is found that for a hydrophilic plate, the vertical force necessary to break the meniscus during removal of the plate from the liquid is larger than the force necessary to break the meniscus during submersion of the plate into the liquid. Furthermore, the capillary force on the plate reaches a maximum before the meniscus collapses during removal, but no maximum exists before collapse during submersion. The reverse is true when the plate is hydrophobic. The study is then extended to investigate the interaction force between two plates, each forming a meniscus with the liquid. The elevations of the plates from the far-field liquid surface are prescribed, in contrast to earlier studies where interaction between long cylinders floating under self weight was considered. Here, the menisci are determined exactly using the Young–Laplace equation. It is shown that for prescribed plate elevations, there can be at most two possible pairs of menisci between them. Each pair bifurcates from a meniscus that is determined by the elevations of the plates and the gap between them. Furthermore, as known for solids floating under self-weight, the horizontal component of the interaction force is attractive for similar menisci (e.g. when the two plates are equally displaced in or out of the liquid), and repulsive when they form opposite menisci. It is shown that if the two menisci are of the same type, but not similar (e.g. one plate is pushed more into the liquid than the other), then the force is attractive at long distances, and may be repulsive at shorter distances with a stable equilibrium at a finite distance between the plates, depending on the elevations of the plates. Such interaction can be between two hydrophilic or two hydrophobic plates or between a hydrophilic and a hydrophobic plate.

1. Introduction

The problem of the meniscus has intrigued scientists for the last two centuries, beginning with Young (1805) and Laplace (1966, first published by Laplace in 1806) who related the curvature of the meniscus to the pressure difference across it. Based on this relation, the shape and stability of the meniscus and the force it exerts on solids have been addressed by several authors (e.g. Poisson 1831). Recent relevant works include those of White & Tallmadge (1965), Concus (1968), Hildebrand & Tallmadge (1970), Padday (1971), Padday & Pitt (1972), Padday, Pitt & Pashley (1975) and Padday *et al.* (1997). These works involve a common mathematical theme –

solving the Young–Laplace equation expressed as a second-order nonlinear ODE, some offering approximate solutions (see e.g. Padday *et al.* 1975 for a historical account), and some offering solutions for specific assumed boundary conditions, e.g. perfect wetting condition (White & Tallmadge 1965; Hildebrand & Tallmadge 1970).

A common physical theme involved in the works of several authors is that a meniscus is formed by a liquid with a macroscopic (thick) hydrophilic solid, e.g. a capillary rise (Concus 1968), a pendant drop from a solid surface (Majumdar & Michael 1976), a liquid bridge between two solid surfaces or a solid surface and the free liquid surface, and a sessile drop (Padday 1971). The edges of the solid formed by the vertical and horizontal surfaces (the horizontal surface is in contact with liquid) are assumed sharp and although the angle (say, with the vertical) of the meniscus at the edge is allowed to change, the mechanism by which the liquid accommodates this change maintaining thermodynamic equilibrium remains unclear.

The effect of the corner of a solid on liquid spreading is studied by Oliver, Huh & Mason (1977) to verify Gibbs' (Gibbs 1906) criterion on the angle of the meniscus near the three-phase (air/liquid/solid) contact line at the edge of a solid. Here, the corners of the axisymmetric solids were varied between 10° and 170°. Following the verification, it was argued that the edge may be considered to have a small finite radius which allows the meniscus to change its angle with the vertical to maintain global equilibrium, while maintaining a fixed local contact angle, a thermodynamic parameter for the given solid/liquid/vapour system. Using this mechanism, i.e. the contact angle is independent of the location of the contact line, Orr, Scriven & Rivas (1975) investigated liquid bridges between two solids using the Young–Laplace equation and showed that the usually expected attractive capillary force between the solids can become repulsive when wetting is imperfect (sum of the contact angles with the solids is greater than π).

An effect of surface tension, known from our everyday experience, is that small floating bodies on liquid/air interfaces attract each other and form clusters. For example, floating cereal flakes on a bowl of milk attract each other, small particles such as ground pepper, glass particles or small pieces of aluminium foil strewn on water attract each other to form clusters.

Bragg & Nye (1947) employed the interaction force between bubbles on a soap solution to form two-dimensional crystals and demonstrated the formation of crystal defects such as dislocations and grain boundaries. The bubble raft demonstration is still popular in courses on dislocations. Motivated by the demonstration, Nicolson (1949) used the linearized Young–Laplace equation to determine the interaction force between two small (less than 3 mm in diameter) floating bubbles. The force was attributed to the perturbed pressure field around one bubble owing to the presence of the other. The surface tension of the liquid/vapour interface played no explicit role in determining the interaction force. It was shown that the interaction force between the bubbles is attractive until they touch each other. Further approach between their centres generates repulsive force owing to the compression of the bubbles. Subsequent refinement of the analysis included the effect of surface tension in determining the interaction force. For example, the force between two long identical cylinders with circular cross-sections, floating in equilibrium under self-weight, was evaluated by Gifford & Scriven (1971), one of the two studies, to the best of our knowledge, that treated the interaction problem between floating bodies without linearizing the Young–Laplace equation. The other study, by Mansfield, Sepangi & Eastwood (1997), investigated the interaction force between long plates, also floating in equilibrium under self weight. The study accounted for the tilt of the plates as they approach

each other. Furthermore, it investigated the phenomenon of floatation of small solid bodies of arbitrary shape due to buoyancy and capillarity, as well as the interaction force between them using the linearized Young–Laplace equation.

The relevance of the interaction between floating bodies to the processing of colloidal materials has prompted a series of studies during the last decade. The major goal of these studies was to investigate the interaction between two floating spheres based on the linearized Young–Laplace equation. For example, Chan, Henry & White (1981) showed that for floating spheres and circular cylinders, the error introduced by linearization is small when the Bond number $B = (\rho_B - \rho_A)gR^2/\gamma_{AB}$ is sufficiently small. Here, A and B are the two media forming the meniscus interface, ρ is the density, R is the radius of the sphere or cylinder, and γ_{AB} is the surface energy of the interface between A and B. The linearized result with small Bond number for two long cylinders was compared with the exact solution obtained earlier by Gifford & Scriven (1971), and close correspondence was observed. A linear analysis on the interaction force between two floating cylinders by Allain & Cloitre (1988) also showed close correspondence with the predictions by the exact analysis when the Bond number is small. The study also provided the conditions necessary for the interaction force to be attractive or repulsive. More recent studies include investigation of the interaction force and energy between two submillimetre sized floating spheres, taking into account the gravitational, wetting and surface energies, using a linearized Young–Laplace equation (Paunov *et al.* 1993). The analysis allowed the spheres to be close to each other as long as the slopes of the menisci are small. Good correspondence was found between the forces predicted by Paunov *et al.* (1993) and Chan *et al.* (1981) when applied to spheres far from each other. The interaction force between a floating sphere and a vertical wall forming a meniscus was studied by Kralchevsky *et al.* (1994) and Velev *et al.* (1994) for shallow menisci, theoretically and experimentally, and it was shown that the force can be both attractive or repulsive, and there can be a stable equilibrium at a finite separation between the wall and the sphere. The interaction force between two spheres in a thin film of liquid supported by a spherical surface is studied by Kralchevsky, Paunov & Nagayama (1995), where one of the motivations was the understanding of the properties of biomembranes containing membrane proteins. A comprehensive review of the interaction between floating bodies on the interface of two fluids has been presented by Kralchevsky & Nagayama (2000).

There has been a growing interest in self-assembly of structures, e.g. monolayers or complex systems from a large number of independent components. The interest is motivated by increasing miniaturization and complexity of engineering systems, and is inspired by the biological world where complex aggregates are formed by molecular self-assembly (Terfort, Bowden & Whitesides 1997). Intriguing patterns with rich structures have been obtained by spontaneous self-assembly of millimetre sized particles such as rotating magnetic disks floating on a liquid subjected to magnetic and hydrodynamic forces (Grzybowski, Stone & Whitesides 2000). Plates of various shapes, made of PDMS (polydimethylsiloxane), floating on the interface between two fluids were found to form stable aggregates. The plates were subjected to interaction force due to surface tension of the interface. The pattern of the aggregates was determined by the shape and size of the plates as well as by the patterned hydrophobicity and hydrophilicity of their sides (Bowden *et al.* 1997, 1999; Choi, Bowden & Whitesides 1999; Bowden *et al.* 2000, 2001*a*, *b*). These parameters in turn influence the shape of the menisci between the plates and hence the interaction force. Grzybowski *et al.* (2001) presented an analytical model (using the linearized Young–Laplace equation) and finite element simulation of the shape of the meniscus and the

interaction energy between two plates. Here, the meniscus was considered pinned at the edge of a plate. Hence, the plate thickness did not play any role in the model except in defining the height of the meniscus. However, the mechanism by which the meniscus changes its angular orientation at the edge at various distances between the plates was not described in the paper.

Recently, micromechanical systems have been widely employed for fluidic applications. They include micro-analytical devices (Warren *et al.* 1999; Manz *et al.* 1990), micro-pumps (Temmel *et al.* 1996; Saif, Alaca & Sehitoglu 1999; Soerensen *et al.* 1999), fluid transport and mixing by micro-channels (Liu *et al.* 2000), liquid micromotors (Kim 1999), and even in micro-fabrication (Kladits & Bright 2000; Syms 1999), to name just a few. Micro-fabricated thin-film structures made of polyimide and polysilicon have been self-assembled by floating them on water and employing the interaction capillary force between them by Hosokawa, Shimoyama & Miura (1996). There is an increasing trend of using micro-actuators to interface with liquids for micromanipulation of objects such as biological species (Sager & Saif 1999; Saif 2000) where a meniscus may form between a solid and the liquid. Many fabrication processes require micro-systems to interface with liquids and form menisci (Bustillo, Howe & Muller 1998; Kuiper *et al.* 2000).

In contrast to earlier applications, micromechanical components forming menisci are more likely to be thin plates with thickness of the order of a micrometre, and with lateral dimensions in the range of a micrometre to hundreds of micrometres. Such plates are less likely to be floating bodies, but they may form menisci with a liquid as part of a micro-system. Thus, their elevations from far-field liquid surface are prescribed. The menisci may have steep slopes and the components forming the menisci may be close to each other. Thus, an analysis that involves linearization of the Young–Laplace equation is not sufficient in determining the forces between solids as well as between the solid and the liquid.

With the new applications in mind, this study investigates the force on a thin solid plate forming a meniscus with a liquid, as well as the interaction force between two plates forming menisci with shallow to steep slopes. The elevations of the plates from the far-field liquid surface are prescribed. The study was motivated by a micromechanical experiment shown in figure 1. It involves a thin rectangular plate, 100 μm long, 20 μm wide, 4 μm thick, made of single crystal silicon and coated with a thin layer of silicon dioxide (hydrophilic with water), attached to a calibrated spring (Sager & Saif 1999). It is brought in contact with the surface of water and a meniscus is formed. The plate is then moved vertically upward until the meniscus breaks. The corresponding force of the meniscus on the plate is obtained from the deformation of the spring and its spring constant. A similar experiment is carried out by pushing the plate into water until the meniscus collapses. Here, a reverse meniscus is formed. It is found that the force required to break the meniscus while pulling the plate above the liquid is higher (12.6 μN) than that (9.6 μN) required to push it into the liquid. The experiment is repeated several times with similar results. If the effect of the vertical plate in determining the forces is ignored, which is reasonable since it occupies only a small portion (3%) of the perimeter, then, at first look, the experimental result appears paradoxical, since the hydrostatic pressure (ρgh) is symmetric with respect to the height of the plate about the far-field liquid surface (acting downward when the plate is above, and upward when it is below the far-field surface). Furthermore, the angle of the meniscus with the horizontal is expected (and can be shown) to be symmetric with respect to height as well. Thus, we can pose the question: what is the source of asymmetry in the meniscus breaking forces, i.e. what is the mechanism

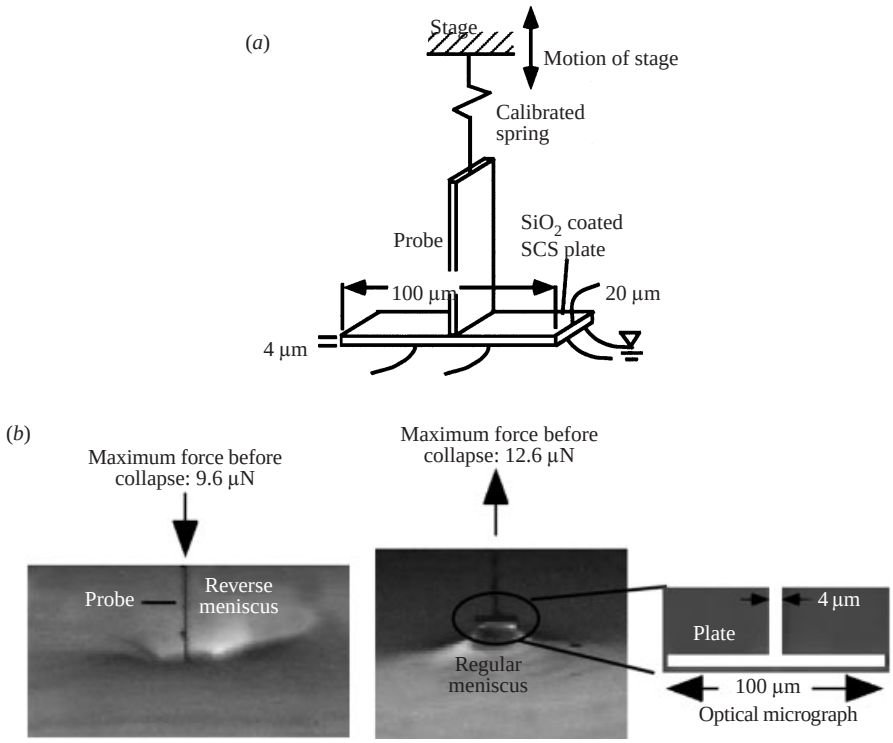

FIGURE 1. (*a*) Diagram of a thin silicon plate, coated by a thin layer of native silicon dioxide (hydrophilic), contacting the surface of water and forming a meniscus. The plate is moved upward/downward by a stage and the force on it is measured by a calibrated spring until the meniscus collapses. (*b*) Optical micrographs of the plate forming menisci with water.

that gives rise to the difference of forces to collapse the two menisci? To address this question, we first explore a mechanism by which a thin rigid solid plate, hydrophilic or hydrophobic, forms a meniscus with a liquid as it moves in (reverse meniscus) or out (regular meniscus) of the liquid. The mechanism is similar to that treated earlier (Gibbs 1906; Oliver *et al.* 1997), by which a liquid wets a corner of a macroscopic solid. Based on this mechanism, the shape of the meniscus and the force that the meniscus applies on the plate for a prescribed admissible displacement of the plate in or out of the liquid surface are obtained from the Young–Laplace relation retaining its nonlinearity.

Next, the interaction force between two neighbouring plates forming menisci with the liquid is investigated. The meniscus between the solids is solved exactly from the Young–Laplace equation, retaining its nonlinearity which allows us to evaluate the interaction force for any gap between the solids, and any admissible heights of the solids above or below the liquid surface. Thus, the analysis captures all possible slopes, shallow to steep, of the meniscus. Note that the study differs from that by Gifford & Scriven (1971) or by Mansfield *et al.* (1997) where the heights of the floating cylinders or plates are determined by their weights. In contrast, here the heights are prescribed. The nonlinear governing equation reveals that there exist bifurcation branches of the solution for the meniscus for prescribed heights of the solids. A physical description is provided for the bifurcation solutions, and the bifurcation points are identified. It is shown that the interaction force between the solids may be attractive at long

distances and repulsive at short distances with a stable equilibrium in between. Such force interaction may be between two hydrophilic or two hydrophobic solids or between a hydrophilic and a hydrophobic solid. Finally, simple desktop experiments are carried out to verify the mathematical predictions. However, first, we outline the basic assumptions adopted in this paper.

2. Assumptions

Let γ_s, γ_{sl} and γ be the interface energies between a solid and a vapour, the solid and a liquid, and the liquid and the vapour respectively, and the three media meet along a line, $\mathscr{L}$. Macroscopically, i.e. outside a core region of radius r_c ($r_c < 100\,\text{Å}$ for most practical purposes (de Gennes 1985)) around $\mathscr{L}$, the liquid meets the solid at a fixed contact angle ϕ and the surface energies are fixed at a static thermodynamic equilibrium condition. They are related by

$$\gamma_{sl} - \gamma_s + \gamma \cos\phi = 0, \tag{2.1}$$

which holds irrespective of the local details of the core region and the curvature of the triple line as long as the radius of curvature is larger than r_c (de Gennes 1985). Within the core region, contact angle and the surface energies can vary.

A pressure differential, Δp, on the two sides of the liquid–vapour interface is related to the principal radii R_1 and R_2 of the interface by

$$\gamma \left(\frac{1}{R_1} + \frac{1}{R_2} \right) = \Delta p, \tag{2.2}$$

which is known as the Young–Laplace equation (Young 1805; Laplace 1966, first published by Laplace in 1806) and is valid as long as R_1, $R_2 \gg r_c$ (de Gennes 1985).

The paper is based on the assumptions that:

(i) All relevant radii, such as the radii of curvature of the surface of the solid plate, and of the triple line $\mathscr{L}$ are much larger than r_c.

(ii) All interfaces are smooth and the local asperities are ignored. Similarly, no local pinning point occurs as the line $\mathscr{L}$ advances along a solid surface.

(iii) The solid plates are long normal to the paper, but they have a finite width. The heights of the meniscus at all points along its length are equal. Thus, the problem is one-dimensional and the meniscus has only one non-zero principal curvature.

3. A long thin solid plate interfacing with a fluid

Consider a long thin rigid strip of a hydrophilic solid ($\phi < \frac{1}{2}\pi$) on the surface of a liquid. Its cross-section at the edge is shown in figure 2(a). For illustration, the plate is assumed symmetric about its vertical axis, and its edge is represented by a semicircle. The outward normal at any point of the boundary is $\bar{n}$.

When brought into contact with the liquid surface, the liquid spreads over the entire bottom of the plate and forms a meniscus. That such a spreading cannot be partial, at least for a circular disk, is shown mathematically by Vogel (1982). If the plate is moved upward, away from the liquid surface, the meniscus takes a form such as shown by m_1 which forms an angle θ_0 with the vertical (positive downward) at $\mathscr{L}$. The vertical component of the capillary force on the plate, contributed from its two edges, is $2\gamma\cos\theta_0$ per unit length of the plate. The force acts downwards. The height of $\mathscr{L}$ from the far-field liquid surface is H_0. As the plate is moved towards the liquid, $\mathscr{L}$ moves upward along the edge of the plate. The corresponding normal, $\bar{n}$, at

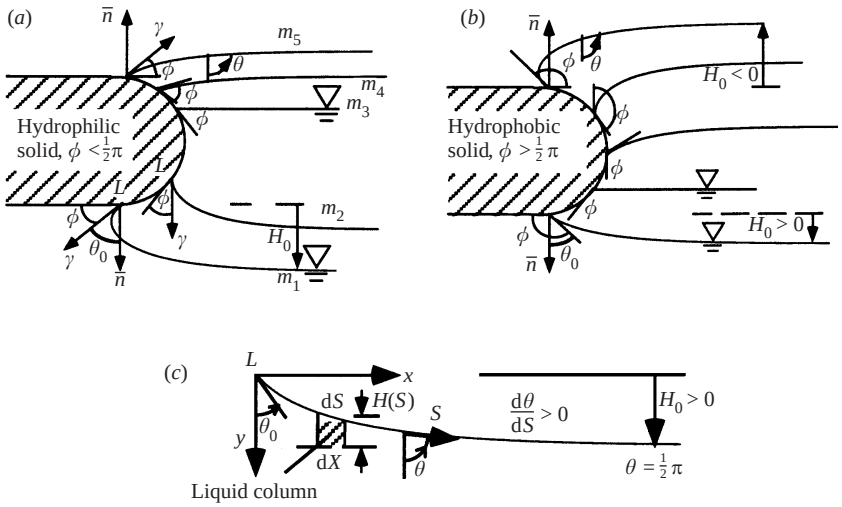

FIGURE 2. (*a*) A family of menisci formed between a hydrophilic solid plate and a liquid is shown for different prescribed heights of the plate. The contact angle ϕ between the tangent to the solid surface and the menisci is constant, but the angle, θ_0, of the meniscus with the vertical at the triple point, $\mathscr{L}$, changes as $\mathscr{L}$ moves from the bottom surface of the plate towards the top with the displacement of the plate towards the liquid. The local normal, $\bar{n}$, to the plate surface rotates from vertical down to vertical up. Among all the members of the family, m_2 offers the maximum capillary force γ (per unit length of triple line) vertically downward. When the plate is lowered into the liquid, m_5 is the highest possible meniscus attainable prior to collapse that offers an upward vertical force $\gamma \sin\phi$, a fraction of γ. (*b*) Similar menisci for a hydrophobic solid. (*c*) The coordinate system used to define the meniscus. All the profiles of the meniscus shown in (*a*)–(*c*) are computed based on the procedure outlined in § 3.4.

$\mathscr{L}$ rotates counterclockwise, but the contact angle remains constant. Such a meniscus is shown by m_2 where $\theta_0 = 0$, and the vertical component of the capillary force is maximum, 2γ, acting downwards. With further downward displacement of the plate, $\mathscr{L}$ gradually moves upward, and θ_0 continues to increase.

For the meniscus m_3, $\theta_0 = \frac{1}{2}\pi$, $H_0 = 0$, and the vertical component of the capillary force on the plate vanishes. The meniscus m_4 corresponds to $\theta_0 > \frac{1}{2}\pi$, and $H_0 < 0$. We refer to the menisci with $\theta_0 > \frac{1}{2}\pi$ as the reverse menisci in contrast to the regular menisci where $\theta_0 \leqslant \frac{1}{2}\pi$. Here, the capillary force offers a vertical component, $|2\gamma \cos\theta_0|$, acting upward per unit length of the plate, which together with the buoyancy force, allows a plate, hydrophilic or hydrophobic, heavier than liquid to float. When $\bar{n}$ becomes vertical, the meniscus forms an angle ϕ with the horizontal (meniscus m_5, compare with figure 1*b*) when $\theta_0 = \frac{1}{2}\pi + \phi$, the maximum value that θ_0 can attain if there is no hysteresis (Carey 1992) in the contact angle. Meniscus m_5 offers the highest possible vertical component of the capillary force acting upward, allowed by the contact angle ϕ and the cross-sectional geometry (horizontal on top) of the plate. Since this upward vertical component, $|2\gamma \cos\theta_0| < 2\gamma$, the downward vertical component for the meniscus m_2, and, as will be shown later, the hydrostatic head at the triple point, $\mathscr{L}$, of m_2 are larger than those of m_5, then the upward force required to break the regular meniscus is larger than the downward force required to break a reverse meniscus for the hydrophilic plate. This explains the source of asymmetry found in the experiment, and is contributed by the hydrophilicity ($\phi < 90°$) of the surface of the experimental plate and its geometric constraint (horizontal top). Symmetry would be retained if $\phi = 90°$.

As the plate is moved up (away from the far-field liquid surface), the menisci go through m_2 when the downward vertical force due to capillarity maximizes, and then decreases with further elevation of the plate until the meniscus m_1 is reached prior to collapse. No such maximum is achieved prior to collapse for the reverse meniscus when the plate is moved downward towards the liquid. Note that the total vertical force due to capillarity and buoyancy may not reach a maximum prior to collapse of the meniscus during the removal of the plate. However, if the width of the plate is small, then the buoyancy force is small compared to the capillary force and the maximum will be reached at a meniscus close to m_2. Such is the case for the small experimental plate, shown in figure 1. If there is hysteresis in the contact angle, then for a hydrophilic plate, the maximum downward capillary force will still be 2γ. However, if $\phi_a > \phi$ is the apparent contact angle for an advancing triple line (Carey 1992), then the maximum upward capillary force prior to submersion is $2\gamma \sin \phi_a$, if $\phi_a < \frac{1}{2}\pi$, or 2γ if $\phi_a \geqslant \frac{1}{2}\pi$. In the latter case, symmetry in the meniscus breaking forces will be restored. Thus, in the absence of hysteresis, $\phi < \frac{1}{2}\pi$ and geometric constraint (horizontal top) give rise to asymmetry. The presence of hysteresis can only reduce the asymmetry (reduce the difference in the meniscus breaking forces), but cannot alone explain the asymmetry. In the rest of the paper, contact angle hysteresis is assumed negligible.

The sequence of menisci for a hydrophobic plate ($\phi > \frac{1}{2}\pi$) for its various heights is shown in figure 2(b). Here, no meniscus is formed when the plate is moved away from the liquid surface.

In order to estimate the force prior to collapse in the experiment of figure 1, we estimate from the micrographs the average angle of the meniscus at the triple points with the vertical as $\theta_0 = 24^\circ$ and 130° corresponding to removal and submersion. Then, with $\gamma = 0.072\,\mathrm{J\,m^{-2}}$ for water, and with a perimeter of 240 μm, the forces for removal and submersion are found to be 15.8 μN and 11.1 μN, respectively. The corresponding experimental values are 12.6 μN and 9.6 μN, respectively. Note that one-dimensional meniscus theory presented in this paper cannot be readily applied to the small-plate experiment where the meniscus has both non-zero curvatures.

3.1. *Condition for flotation*

It is well known that buoyancy and the vertical component of the capillary force allow small solids to float on liquids. The condition for floatation of a long plate with thickness t, width $2W$ and density ρ_s can be readily written as

$$\gamma \sin \phi + W \rho_l g H_0 \geqslant W t g(\rho_s - \rho_l), \tag{3.1}$$

where ρ_l is the density of the liquid and H_0 is the depth of the triple line (i.e. the top surface of the plate). For a circular plate with radius r, the condition for floatation becomes

$$2\pi\gamma \sin \alpha_0 + \pi r \rho_l g H_0 \geqslant \pi r t g(\rho_s - \rho_l), \tag{3.2}$$

where α_0 is the maximum possible angle that the meniscus can make with the horizontal when the locus of the triple line is a circle (instead of a straight line in the case of a long plate), and H_0 is the corresponding depth of the triple point. Thus, however large the quantity $g(\rho_s - \rho_l)$ may be, for a given upper bound of the left-hand sides of (3.1) and (3.2), we can always find a small enough Wt or rt so that the condition for flotation is satisfied. In other words, a small enough solid plate, hydrophilic or hydrophobic, no matter how dense it is, can float in any gravitational field, as long as the radius of curvature of the solid surface is larger than r_c, the radius

of the core region of the triple point. It is, however, worth noting that circular thin plates are difficult to fabricate when micro mechanical systems are formed by deep etching (such as deep silicon etching) or by filling a mould.

A mathematical model is provided next.

3.2. *Mathematical modelling*

We start by setting up the coordinates shown in figure 2(*c*). The triple point, $\mathscr{L}$, is the origin, Y denotes the vertical axis (positive downward), S is the coordinate along the liquid–vapour interface, $\theta(S)$ is the angle that the tangent to the interface makes with the vertical at S. For the one-dimensional meniscus, the Young–Laplace equation (equation (2.2)) can be represented as

$$\frac{\mathrm{d}\theta}{\mathrm{d}s} = h_0 - y \quad \text{with} \quad \theta(s=0) = \theta_0, \tag{3.3}$$

which has been non-dimensionalized by the capillary length $l_0 = \sqrt{\gamma/\rho g}$. Here, in reference to (2.2), $1/R_1 = \mathrm{d}\theta/\mathrm{d}S$, $1/R_2 = 0$, $\Delta p = \rho g(H_0 - Y)$, the hydrostatic pressure assuming that the atmospheric pressure does not change with the small height of the meniscus, ρ is the density of the liquid, and $S = sl_0$, $H_0 = l_0 h_0$ and $Y = l_0 y$. Note that the small letters, such as s, h and y, denote lengths non-dimensionalized by l_0. For a given h_0, θ_0 must be such that the meniscus at the far field becomes horizontal, i.e. as $s \to \infty$, then $\mathrm{d}\theta/\mathrm{d}s \to 0$, and $\theta \to \frac{1}{2}\pi$. In order to solve (3.3), we take the derivative of both sides with respect to s, multiply by $\mathrm{d}\theta/\mathrm{d}s$, and integrate with respect to s to obtain

$$\tfrac{1}{2}\theta'^2 + \sin\theta = \tfrac{1}{2}h_0^2 + \sin\theta_0 = 1 \tag{3.4}$$

where we use $\mathrm{d}y/\mathrm{d}s = cos\theta$, $\theta'(s=0) = h_0$, and $\theta'(\theta = \frac{1}{2}\pi) = 0$. Here, $'$ denotes derivative with respect to s. Equation (3.4) gives the relation between h_0 and θ_0:

$$h_0 = \pm\sqrt{2}\sqrt{1 - \sin\theta_0} = 2\sin\beta_0, \tag{3.5}$$

where $\beta_0 = \frac{1}{4}\pi - \frac{1}{2}\theta_0$. h_0 is positive when $-\frac{3}{2}\pi \leqslant \theta_0 \leqslant \frac{1}{2}\pi$ or $0 \leqslant \beta_0 \leqslant \pi$, and h_0 is negative when $\frac{1}{2}\pi \leqslant \theta_0 \leqslant \frac{5}{2}\pi$ or $-\pi \leqslant \beta_0 \leqslant 0$, i.e. the sign of $\sin\beta_0$ is similar to that of h_0, which is the reason for introducing the angle β_0. Equation (3.5) implies that $h_0 = H_0/l_0$ can vary between -2 and $+2$ for all solids (hydrophilic and hydrophobic) and liquids under any gravity. For a given ϕ, the geometry of the edge determines the possible range of θ_0 and hence h_0. For the flat plate of figure 2(*a*, *b*), θ_0 can vary from $-(\frac{1}{2}\pi - \phi)$ to $(\frac{1}{2}\pi + \phi)$. If the edge is circular then the range increases, although the contact angle (ϕ) remains the same. Thus, a hydrophilic or a hydrophobic solid can be designed to contact a liquid surface and move into the liquid without submerging itself, which offers micro actuators considerable flexibility for manipulating objects in liquids with a probe. For example, a thin plate attached to an actuator in air can form the meniscus preventing the liquid from wetting the actuator, whereas the probe attached to the plate may be inundated (figure 3).

3.3. *Uniqueness of the solution for the meniscus*

PROPOSITION. *For a prescribed admissible height, h_0, of the triple point, there may be only two possible menisci.*

Proof. Let the prescribed non-dimensional height of the triple point $\mathscr{L}$ be $h_0 > 0$ (i.e. only the positive solution in (3.5) is considered). Then $\theta_0 < \frac{1}{2}\pi$. Now, if $-\frac{1}{2}\pi \leqslant$

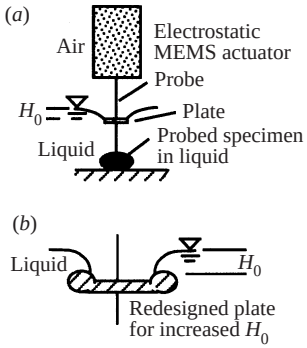

FIGURE 3. (*a*) A thin solid plate attached to a hydrophilic actuator forms a meniscus with a liquid when it is pushed into the liquid. The plate allows a probe to interact with a specimen in the liquid while keeping the hydrophilic actuator dry. (*b*) The plate boundary can be designed to increase the allowable range of the displacement of the probe into the liquid.

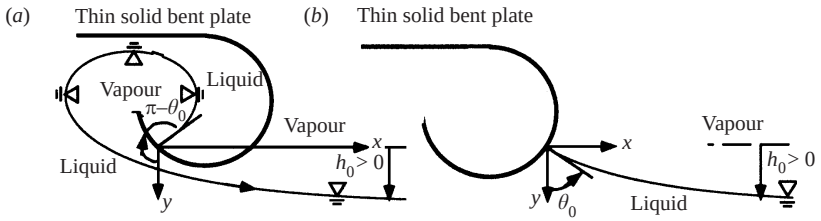

FIGURE 4. Two possible menisci between a solid and a liquid for a prescribed height of the triple point. Here, $h_0 > 0$, and the initial angle of the meniscus with the vertical is θ_0 and $-\pi - \theta_0$, both satisfying (3.5). The two menisci merge when $\theta_0 = -\frac{1}{2}\pi$, i.e. $h_0 = 2$. The bent plates are introduced to illustrate the multiplicity of menisci for a given height of the triple point. The profiles of the menisci are computed based on the procedure outlined in § 3.4.

$\theta_{01} < \frac{1}{2}\pi$ satisfies (3.5) then so does $\theta_{02} = -\pi - \theta_{01}$ (figure 4). Thus, the menisci, m_{01} or m_{02}, starting with $\theta_0 = \theta_{01}$ or $\theta_0 = \theta_{02}$ increase θ from θ_0 to $\frac{1}{2}\pi$ with increasing s. There are other angles $< -\frac{3}{2}\pi$, such as $\theta_{03} = -2\pi + \theta_{01}$ that also satisfy (3.5), but a meniscus starting with $\theta_0 = \theta_{03}$ increases θ to $\theta = -\frac{3}{2}\pi$ as $s \to \infty$ which results in a meniscus m_{03} identical to m_{01}. Similarly, the meniscus with $\theta_0 = -2\pi - \theta_{01}$ coincides with m_{02}. Thus, for a given h_0 there are two distinct menisci. They merge into one when $\theta_0 = -\frac{1}{2}\pi$ or $h_0 = 2$ by (3.5), and we can view the two menisci as the two bifurcation branches with $\theta_0 = -\frac{1}{2}\pi$ as the bifurcation point. Similarly, when $h_0 < 0$, there may be at most two possible menisci.

3.4. *Profile of the meniscus*

The meniscus profile in (s, θ) coordinates is obtained from (3.4) with $\beta = \frac{1}{4}\pi - \frac{1}{2}\theta$:

$$\theta'^2 = 2(1 - \sin\theta) = 4\sin^2\beta \quad \text{or} \quad \theta' = 2\sin\beta, \tag{3.6}$$

where only the positive sign is retained for θ', since when $-\frac{3}{2}\pi \leqslant \theta \leqslant \frac{1}{2}\pi$ i.e. $0 \leqslant \beta \leqslant \pi$, and $\sin\beta \geqslant 0$, then the height of the meniscus $h = h_0 - y \geqslant 0$ (follows from (3.5)) and by (3.3), $\theta' \geqslant 0$. Similarly, when $\frac{1}{2}\pi \leqslant \theta \leqslant \frac{5}{2}\pi$ i.e. $-\pi \leqslant \beta \leqslant 0$, then $\theta' \leqslant 0$. Thus, the signs of θ' and $\sin\beta$ are similar. Carrying out the integration with the limits (θ_0, θ) and $(0, s)$, the relation between s and θ is obtained:

$$\theta = \tfrac{1}{2}\pi - 4\tan^{-1}[\mathrm{e}^{-s}\tan(\tfrac{1}{2}\beta_0)]. \tag{3.7}$$

The x and y coordinates of the meniscus can be obtained in parametric form from $\mathrm{d}x = \sin\theta \mathrm{d}s$ and $\mathrm{d}y = \cos\theta \mathrm{d}s$ with θ or s as parameters:

$$x = \ln\left[\frac{\tan(\frac{1}{2}\beta_0)}{\tan(\frac{1}{2}\beta)}\right] + 2(\cos\beta_0 - \cos\beta), \quad y = 2(\sin\beta_0 - \sin\beta), \tag{3.8}$$

which verify the limits: $\theta = \frac{1}{2}\pi$, $\theta' = 0$, $y = h_0$ and $x \to \infty$ when $s \to \infty$. If $\theta_0 < 0$ or $\theta_0 > \pi$, then the meniscus necks or narrows as s increases from the triple point. The width of the meniscus is minimum at $\theta = 0$ or $\theta = \pi$. The vertical force on the plate is given by the capillary component $2\gamma\cos\theta_0$ plus the buoyancy force that can be obtained from the geometry of the plate and H_0.

Note that the profile of the one-dimensional meniscus formed between a vertical plate partially submerged in a liquid is solved exactly in Cartesian coordinates in text books. e.g. (Batchelor 1967; Carey 1992) where θ_0, the angle with the vertical, is the contact angle, ϕ, and H_0 is the capillary rise at the plate surface. Thus, θ_0, and hence H_0, are fixed for a given combination of liquid, solid and vapour, and a gravitational field. In contrast, (3.8) represents the meniscus formed by a horizontal plate, where θ_0, the angle with the vertical, is arbitrary. It depends on the prescribed height of the triple point which is determined by the prescribed height of the plate.

3.5. *An analogy with elastica*

Consider a semi-infinite slender cantilever beam supported at one end, A, with an angle θ_0 with the vertical. A horizontal force P is applied on the beam far from A. The beam bends, and far away from A its tangent becomes horizontal where the height of the beam is H_0 below the support. The equation governing the deformation of the elastica is given by the moment curvature relation (Popov 1976):

$$\frac{\mathrm{d}\theta}{\mathrm{d}S} = \frac{P}{EI}(H_0 - Y), \quad \theta(S = 0) = \theta_0, \tag{3.9}$$

which is identical to the equation governing the meniscus. They both take the same non-dimensional form (equation (3.3)) $\mathrm{d}\theta/\mathrm{d}s = (h - y)$, $\theta(s = 0) = \theta_0$, the former being non-dimensionalized by $l_0 = \sqrt{EI/P}$ and the latter by the capillary length $l_0 = \sqrt{\gamma/\rho g}$. Thus, in the non-dimensional space, the profiles of the meniscus and that of the elastica are identical (see also Maxwell 1878) when they have the same initial condition $\theta(s = 0) = \theta_0$.

4. Interaction between thin plates forming menisci

In the rest of the paper, the interaction force between two thin solid plates on the surface of a liquid is considered. The heights of the solids (above or below the far-field liquid surface) are prescribed, i.e. an external agent holds the plates at prescribed heights forming a regular or reverse meniscus. The question of interest here is the interaction force between the plates along the horizontal direction for different horizontal gaps between them.

Figure 5 shows various menisci formed between two solids and a liquid. Such menisci can be grouped into two mutually exclusive (will be shown later) families, one in which the meniscus between the two solids has a point that is at the level of the far-field liquid surface. At this point, the curvature of the meniscus vanishes, $\mathrm{d}\theta/\mathrm{d}s = 0$ (figure 5*a*, *b*). The other family consists of menisci that contain a point with height $h_0 = H_0/l_0$ where the tangent to the meniscus becomes horizontal and

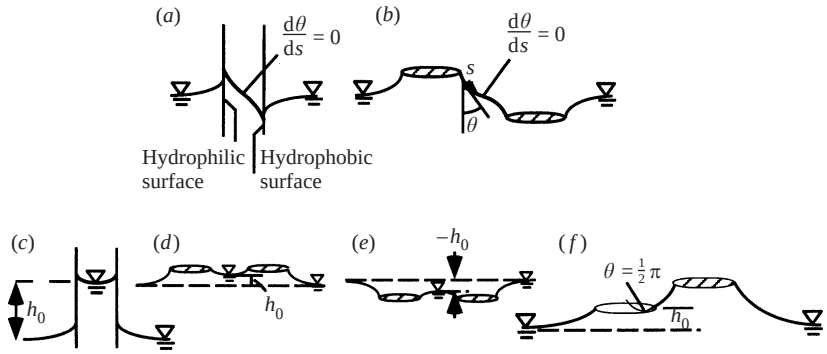

FIGURE 5. A variety of one-dimensional menisci formed between two solids, hydrophilic or hydrophobic. They are categorized into two families: one in which there is a point on the meniscus where the height of the liquid coincides with that of the far field and hence the curvature ($d\theta/ds$) vanishes (*a* and *b*), the other has a point where the tangent to the meniscus (or its extrapolation) becomes horizontal (*c–f*). All distances are non-dimensionalized by the capillary length l_0.

liquid is below this point (figure 5*c–f*). If the point is between the two solids, then it is either above or below the far-field liquid surface, i.e. $|h_0| > 0$. $h_0 = 0$ would imply that the two solids are infinitely far apart from one another and hence there is no interaction between them. The point where the tangent is horizontal may not physically exist between the two solids, but may be obtained by an extrapolation of the meniscus between the solids, as shown in figure 5(*f*).

4.1. *Meniscus between the two solids with* $d\theta/ds = 0$

Figure 6(*a*) shows a meniscus between two solids in a space non-dimensionalized by $l_0 = \sqrt{\gamma/\rho g}$ and is defined by the (s, θ) coordinate system. At $s = 0$, $\Delta p = 0$ and $d\theta/ds = 0$. Let $\theta(s = 0) = \theta_0$. The horizontal (positive towards right) and the vertical (positive downward) distances from $s = 0$ are denoted by x and y, respectively. The meniscus satisfies equation (3.3)

$$\frac{d\theta}{ds} = -y, \quad \theta(s = 0) = \theta_0, \tag{4.1}$$

where $-\frac{1}{2}\pi \leqslant \theta_0 \leqslant \frac{1}{2}\pi$ is yet to be determined from the prescribed heights, h_1 and h_2, of the triple points and hence of the plates if they are thin, and the gap, x_0, between them. For a given θ_0, the meniscus is completely defined, and the two solids can be placed at any pair of points on it as long as the solids provide a surface that allows us to preserve the solid–liquid contact angle, ϕ, shown in figure 6(*a*). Here, a possible location of the left solid is shown by dotted lines. The solution of (4.1) is symmetric with respect to $y = 0$ and can be obtained by treating the problem such that if both the solids are below the far-field liquid surface ($y > 0$) at $s = s_1$ and $s = s_2$, $s_1, s_2 \geqslant 0$. Differentiating both sides of (4.1) with respect to s, multiplying by θ', and integrating with respect to s in $(0, s)$ we obtain

$$\theta' = -\sqrt{2(\sin\theta_0 - \sin\theta)}, \tag{4.2}$$

where $\theta'(s = 0) = 0$, $\theta(s = 0) = \theta_0$ are used. The negative root is retained since when $y > 0$, $\theta' < 0$ (equation (4.1)). Equations (4.1) and (4.2) give the relation between the height of the meniscus $h = y$ and the corresponding θ, i.e.

$$h = \sqrt{2(\sin\theta_0 - \sin\theta)}, \quad h_i = \sqrt{2(\sin\theta_0 - \sin\theta_i)}, \tag{4.3}$$

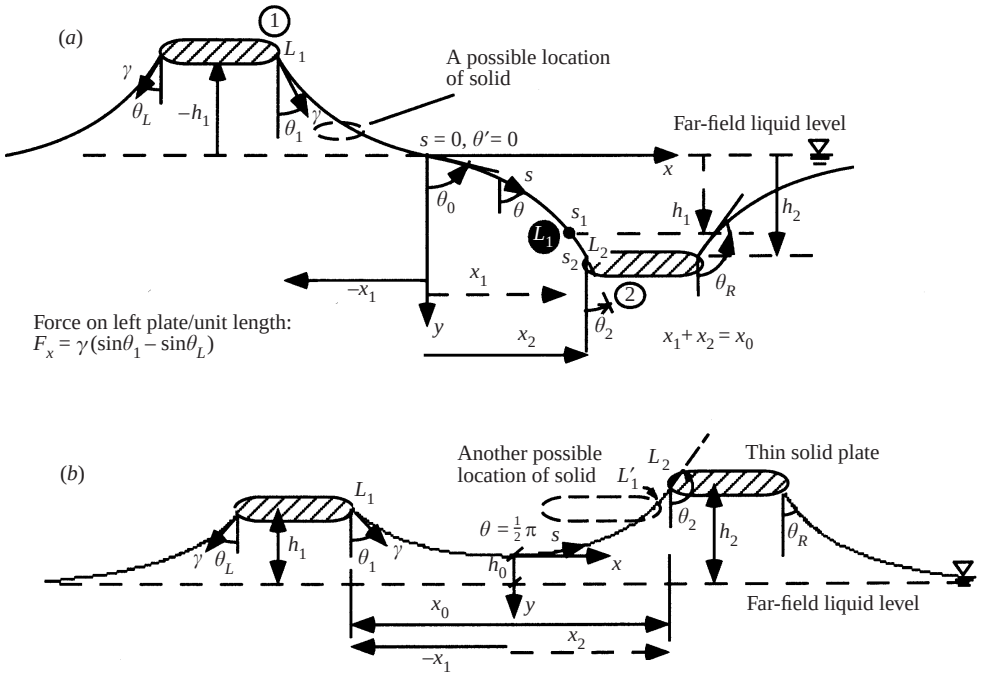

FIGURE 6. (*a*) A meniscus between two thin solid plates, one above and the other below the far-field liquid surface. The meniscus has a point where the curvature vanishes, $\mathrm{d}\theta/\mathrm{d}s = 0$. The coordinate system is shown. The image of the triple point $\mathscr{L}_1$ (point 1, above the far-field liquid surface) is shown by a shaded circle 1 below the far-field liquid surface. (*b*) A meniscus between two solid plates above the far-field liquid surface. For given heights h_1 and h_2 of the solids, two menisci, $\mathscr{L}_1\mathscr{L}_2$ or $\mathscr{L}'_1\mathscr{L}_2$ are shown. $\mathscr{L}_1\mathscr{L}_2$ or an extrapolation of $\mathscr{L}'_1\mathscr{L}_2$ has a point where the tangent becomes horizontal. The origin of the coordinate system is chosen at this point. $\mathrm{d}\theta/\mathrm{d}s \neq 0$ in $\mathscr{L}_1\mathscr{L}_2$ or $\mathscr{L}'_1\mathscr{L}_2$. All distances are non-dimensionalized by the capillary length l_0.

where $\theta = \theta_i$ at $\mathscr{L}_i$. The horizontal distance, $x_0 = x_1 + x_2$, between $\mathscr{L}_1$ and $\mathscr{L}_2$ is

$$x_0 = \int_0^{s(\theta_1)} \sin\theta \mathrm{d}s + \int_0^{s(\theta_2)} \sin\theta \mathrm{d}s = \int_{\theta_0}^{\theta_1} \sin\theta \frac{\mathrm{d}\theta}{\theta'} + \int_{\theta_0}^{\theta_2} \sin\theta \frac{\mathrm{d}\theta}{\theta'}, \tag{4.4}$$

where $\theta'(\theta_0, \theta)$ is given by (4.2). Since by (4.3), $\theta_i = \theta_i(h_i, \theta_0)$, then (4.4) contains the only unknown θ_0, for given h_1, h_2 and x_0, thus providing the necessary condition to solve for θ_0. Once θ_0 is obtained, the meniscus $\mathscr{L}_1\mathscr{L}_2$ can be defined as $\theta = \theta(s)$ by integrating (4.2):

$$\int_{\theta_0}^{\theta} \frac{\mathrm{d}\theta}{-\sqrt{2(\sin\theta_0 - \sin\theta)}} = s. \tag{4.5}$$

The left-hand side is an elliptic integral of first kind, hence the integration must be carried out numerically. θ_i, $i = 1, 2$, can then be obtained from (4.3) using θ_0 and h_i, $i = 1, 2$.

Bounds on h_i

From (4.3), $|h_i| \leqslant 2$. $h_i = 2$ when $\theta_0 = \frac{1}{2}\pi$ and $\theta_i = -\frac{1}{2}\pi$. For a given θ_0, the maximum value that h_i can attain is determined by $\frac{1}{2}h_i^2 = 1 + \sin\theta_0$.

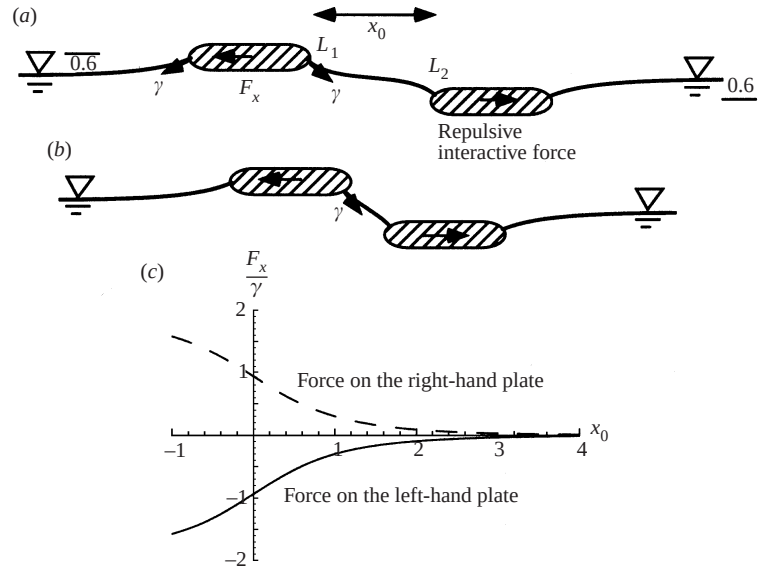

FIGURE 7. (a, b) Computed (§ 4.1) menisci between two plates, one above and one below the far-field liquid surface by 0.6 are shown for two different non-dimensional gaps, x_0, between the plates. The outer menisci are computed based on the procedure outlined in § 3.4. The horizontal force (per unit length of the plates normal to the paper) on each plate owing to the proximity of the other is shown in (c). The forces are equal and opposite. The interaction force is repulsive between the plates at all distances. Here, the spatial dimensions are normalized by the capillary length $l_0 = \sqrt{\gamma/\rho g}$. Thus, the actual distance between the plates $= x_0 l_0$.

4.2. *Interaction force between the plates*

The horizontal force, F_x, per unit length of each plate (normal to the paper) in figure 6 is given by

$$F_x = \gamma(\sin\theta_1 - \sin\theta_L). \tag{4.6}$$

Here, θ_L is determined from (3.5) where θ_0 is replaced by θ_L. θ_1 is determined by the procedure outlined in § 4.1. When the plates are far apart, $\theta_L = \theta_1$ by symmetry, and $F_x = 0$. As the plates approach each other, the symmetry is lost, and the interaction force appears.

Figure 7 shows the menisci (computed) formed by two thin plates with $h_1 = -0.6$ and $h_2 = 0.6$, and their interaction force, F_x/γ, for various gaps, x_0, between them. Here the left-hand and right-hand solids are subjected to equal forces towards the left and right, respectively, i.e. the interaction force is repulsive. The equal and opposite forces satisfy system equilibrium, a condition which was not explicitly enforced in deriving the meniscus, and thus provides an independent check of the evaluation of the meniscus. It is important to note that since the derivation of the meniscus does not involve linearization of the Young–Laplace equation (equation (2.2)), hence the meniscus slopes can be large.

The physical mechanism by which the repulsive force appears can be seen as follows. As the plates approach each other, the tangents to the meniscus at $\mathscr{L}_1$ and $\mathscr{L}_2$ incline towards the vertical direction. Thus, the horizontal component of the capillary force on the plates at $\mathscr{L}_1$ and $\mathscr{L}_2$ decreases. However, the menisci on the outer edges of the plates remain unchanged, i.e. the horizontal component of the surface tension remain unchanged. Consequently, the plates are subjected to horizontal forces away from

each other, i.e. they repel each other. Thus, solids forming opposite menisci repel each other.

4.3. *Meniscus between the two solids with* $\mathrm{d}\theta/\mathrm{d}s \neq 0$

Figure 6(*b*) shows a possible meniscus, $\mathscr{L}_1\mathscr{L}_2$ between two thin solids with non-dimensional heights h_1 and h_2 from the far-field liquid surface. Two possible locations of the solid on the left-hand side are shown with triple points $\mathscr{L}_1$ and $\mathscr{L}'_1$, both with height h_1. The hydrostatic head does not vanish in $\mathscr{L}_1\mathscr{L}_2$ or $\mathscr{L}'_1\mathscr{L}_2$. The tangent to the meniscus becomes horizontal, i.e. $\theta = \frac{1}{2}\pi$ at a point on $\mathscr{L}_1\mathscr{L}_2$ or at a point on the curve extrapolated from $\mathscr{L}'_1\mathscr{L}_2$. We choose the origin $s = 0$ at the point where the tangent is horizontal. Let the height of the meniscus at $s = 0$ be h_0 in non-dimensionalized units. The gap between $\mathscr{L}_1$ and $\mathscr{L}_2$ is x_0. The horizontal distance from $s = 0$ is given by x, and the vertical distance by y. Note that when $h_0 > 0$, the point $s = 0$ is elevated above the far-field liquid surface, and $\theta' = \mathrm{d}\theta/\mathrm{d}s > 0$ for all s in $\mathscr{L}_1\mathscr{L}_2$. Thus, h_1, $h_2 > h_0$. The entire meniscus is then elevated above the far-field liquid level, and $s = 0$ is the lowest point. Similarly, when $h_0 < 0$, $\mathscr{L}_1\mathscr{L}_2$ is depressed below the far-field liquid surface with $s = 0$ as the highest point. Thus, for either case ($h_0 > 0$ or $h_0 < 0$), h_0 and the corresponding h_i are of the same sign and $|h_i| > |h_0|$. Also, $|\theta'| > 0$ at all points of $\mathscr{L}_1\mathscr{L}_2$, and the signs of θ' and h_0 are similar.

The governing equation for the meniscus (figure 6*b*) is

$$\frac{\mathrm{d}\theta}{\mathrm{d}s} = h_0 - y, \quad \theta(s = 0) = \tfrac{1}{2}\pi, \tag{4.7}$$

For given h_0, the meniscus is completely defined. However, h_0 is as yet unknown and can be obtained from the prescribed x_0 between $\mathscr{L}_1$ and $\mathscr{L}_2$. Differentiating both sides of (4.7) with respect to s, multiplying by θ', and integrating with respect to s in $(0, s)$ we obtain

$$\theta' = h_0\sqrt{1 + \frac{2}{h_0^2}(1 - \sin\theta)}, \tag{4.8}$$

where $\theta(s = 0) = \frac{1}{2}\pi$ and $\theta'(s = 0) = h_0$ by (4.7) are used. Here, only the positive sign of the square root is retained since the sign of θ' and h_0 are similar. From (4.7), at $\mathscr{L}_i$, $i = 1, 2$,

$$\theta'(\text{at } \mathscr{L}_i) = h_0 - y = h_i, \tag{4.9}$$

which together with (4.8) gives the relation between h_i and θ_i:

$$h_i = h_0\sqrt{1 + \frac{2}{h_0^2}(1 - \sin\theta_i)}. \tag{4.10}$$

The horizontal gap, x_0, between $\mathscr{L}_1$ and $\mathscr{L}_2$ can then be represented as a function of h_0 as follows:

$$x_0 = \int_{\pi/2}^{\theta_2} \sin\theta \mathrm{d}s + \int_{\theta_1}^{\pi/2} \sin\theta \mathrm{d}s = \int_{\pi/2}^{\theta_2} \sin\theta \frac{\mathrm{d}\theta}{\theta'} + \int_{\theta_1}^{\pi/2} \sin\theta \frac{\mathrm{d}\theta}{\theta'}, \tag{4.11}$$

where $\theta'(\theta, h_0)$ and $\theta_i(h_i, h_0)$ are given by (4.8) and (4.10) respectively. Thus, h_0 can be solved numerically from (4.11) for given h_i and x_0. θ_i, $i = 1, 2$, then follow from (4.10) and the profile of the meniscus $\mathscr{L}_1\mathscr{L}_2$ ((s, θ) coordinates) can be obtained from (4.8)

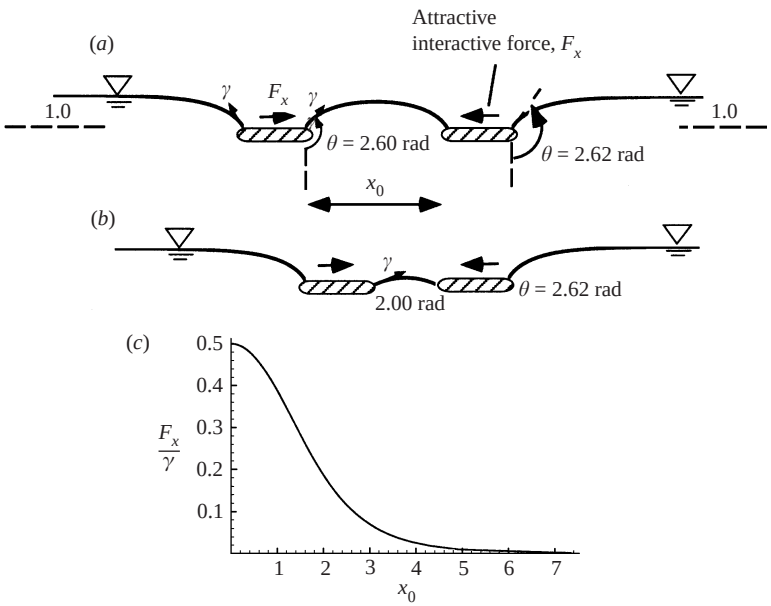

FIGURE 8. Interaction between two thin solid plates, both pushed into the liquid by normalized height $h = -1$. Actual height $= l_0 h$, where l_0 is the capillary length $= \sqrt{\gamma/\rho g}$. The menisci formed by the solids at two different non-dimensional gaps, x_0, between the solids are shown in (a) and (b). They are computed based on the procedures outlined in §§ 3.4 and 4.3. The interaction force is shown in (c). The force is attractive at all distances, since the direction of the capillary force, γ, between the two plates aligns along the horizontal direction as the plates approach each other.

by a numerical integration:

$$\int_{\pi/2}^{\theta} \frac{\mathrm{d}\theta}{h_0\sqrt{1+(2/h_0^2)(1-\sin\theta)}} = s. \tag{4.12}$$

The interaction force is given by (4.6).

Figures 8(a) and 8(b) show the menisci between two thin plates, both with $h_1, h_2 = -1$, as they approach each other. The interaction force (figure 8c) is attractive for all distances between the plates. As the distance between the plates decreases, the meniscus between them aligns more with the horizontal. Thus, the horizontal component of the capillary force at $\mathscr{L}_1$ and $\mathscr{L}_2$ increases compared to the horizontal components of the outer menisci. The attractive interaction force thus increases as they approach.

Figures 9(a)–9(c) show the menisci between two solids as they approach each other with $h_1 = -0.5$ and $h_2 = -1$. Figure 9(d) shows the interaction force. At large distances, θ_1 and θ_L for the solid on the left-hand side are equal, and the horizontal force vanishes. As the solids approach each other, θ_1 decreases and the horizontal force to the right increases. At state A, $\theta_1 = \frac{1}{2}\pi$ where the force towards right is maximum, $\gamma(\sin(\frac{1}{2}\pi) - \sin\theta_L)$. With further approach, θ_1 continues to decrease resulting in a decrease of force to the right. At state B, $\theta_1 = \pi - \theta_L$ and the force vanishes ($\sin\theta_L - \sin(\pi - \theta_L) = 0$). During this approach, θ_2 decreases from θ_R, goes through a minimum at state A and returns to $\theta_2 = \theta_R$ at state B. With further approach, θ_1 decreases below $\theta_1 = \pi - \theta_L$ and θ_2 increases beyond θ_R, when the force becomes repulsive. Thus, the interaction force is attractive at long distances, repulsive at short distances, and has a stable equilibrium at a finite distance between the two

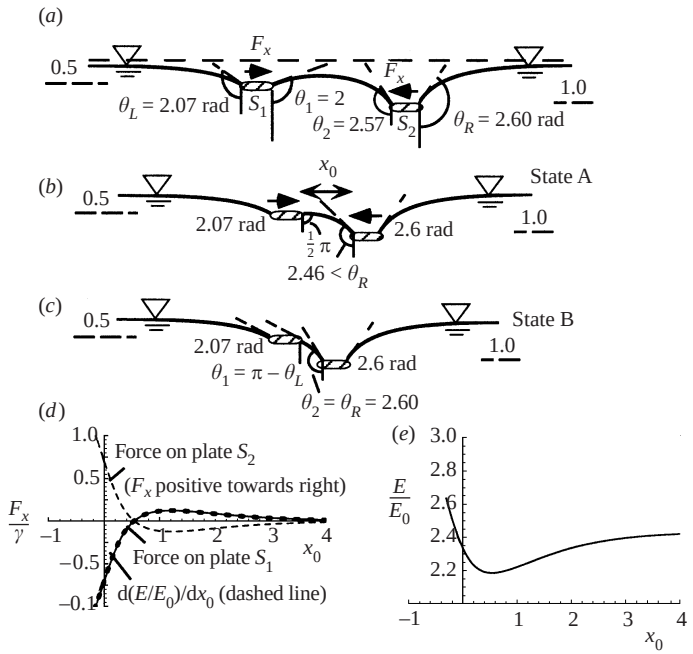

FIGURE 9. Interaction between two thin solid plates, pushed into the liquid by normalized heights $h = -0.5$, and -1. Actual height $= l_0 h$ where l_0 is the capillary length $= \sqrt{\gamma/\rho g}$. The menisci at three different gaps, x_0, between the solids are shown in (*a*)–(*c*). The profiles of the two outer menisci are computed by the method described in § 3.4 and the meniscus between the two solids by that described in § 4.3. The interaction force, shown in (*d*), is attractive at long distances, repulsive at short distances with a stable equilibrium in between. The force is maximum at state A, and it vanishes at state B. The normalized energy, E/E_0, where $E_0 = l_0\gamma$, due to the hydrostatic head and the surface energy of the meniscus, as a function of x_0 is shown in (*e*). Here, the non-dimensional widths of the plates is 2. A numerical derivative of E/E_0 with respect to x_0 using a linear interpolation between the energy values is calculated. The derivative coincides with the force plot.

solids. The nature of the interaction force depends on the relative magnitudes of h_1 and h_2. When $h_1 = h_2$, the force is only attractive, and the maximum is reached when $x_0 = 0$. When $h_1 \neq h_2$, the maximum is reached at a finite $x_0 > 0$. The force then decreases with a decrease of x_0. At $x_0 = 0$, the force is attractive when h_1 and h_2 are close to each other, but the attraction decreases and may become repulsive with increasing difference between h_1 and h_2, as demonstrated in figure 9. The nature of the interaction force is similar when $h_i, h_0 < 0$.

Bounds on h_i

From (4.10), we have

$$h_i^2 - h_0^2 = 2(1 - \sin\theta_i).$$

Since $2 \geqslant 1 - \sin\theta_i \geqslant 0$, hence $4 \geqslant h_i^2 - h_0^2 \geqslant 0$. Thus, $h_i^2 \geqslant h_0^2 \geqslant h_i^2 - 4$ for $i = 1, 2$. For example, if $h_2 > h_1$ then the domain of h_0^2 is in $(h_2^2 - 4, h_1^2)$.

4.4. *Mutually exclusive families of menisci*

PROPOSITION. *The two families of menisci, one with $\theta' = 0$ and the other with a point A where the tangent is horizontal and the liquid is below A are mutually exclusive.*

Proof. For the latter family, $0 < |h_0| < |h|$ at any point on the meniscus where h_0 is the height of the meniscus at A and h is the height at any point of the meniscus. Also, h_0 and h have the same sign. Thus, A is the lowest or the highest point of the meniscus. Then, by (4.7), where y and h_0 have opposite signs, $\theta' \neq 0$ at any point on the meniscus. For the former family, let $\theta' = 0$ at B on the meniscus. Then, $h(B) = 0$ and $\theta(B) \neq \frac{1}{2}\pi$. At any point of the meniscus below the far-field liquid surface, $\theta' < 0$ and above the far-field liquid surface, $\theta' > 0$ (equation (4.1)). Thus, if there exists a point, A', on the meniscus where the tangent is horizontal, then the liquid is above A' (see e.g. figure 10). Thus, the two families are mutually exclusive.

4.5. *Formation of clusters by floating plates: is there a critical size for sinking?*

Solids, floating on liquids, are known to agglomerate owing to interaction forces between them. The shape and size of a cluster formed by floating plates depend on the size and shape of the plates and their initial states. The weight of the cluster is the sum of the weights of the individual plates, but the perimeter of the cluster is less than the sum of the perimeters. Thus, it appears at first look that, as agglomeration proceeds, the cluster should soon reach a critical size above which it should sink. The critical size should roughly be the maximum size of an equivalent single plate of similar shape that can float by buoyancy and capillarity. However, let us consider an alternative scenario. It is known (Mansfield *et al.* 1997) that as the plates agglomerate, they also tilt. Thus, in a cluster, the plates surrounded by other plates lower their elevation, while the outer plates gradually increase their elevation by tilting. The inner plates are supported primarily by buoyancy, the outer plates by buoyancy and capillarity. Thus, with agglomeration, the total hydrostatic force increases not as a function of area, but at a rate faster than the rate of increase of area. This raises the question, does there exist a critical size for sinking for a cluster, i.e. can individual units floating by buoyancy and capillarity form a cluster with unbounded size? The difference between a cluster and an individual critical-sized plate is that the plate has high rigidity against bending that prevents it from forming a boat to increase the buoyancy, whereas for the cluster, the absence of moment rigidity at the junction between the plates may allow the cluster to take the required shape for floatation. The topic will be treated in detail in a future publication.

4.6. *Desktop experiments*

Attraction between small floating bodies can be verified from everyday experience such as the attraction between tea particles, ground pepper or small pieces of aluminium foil strewn on water surface. To demonstrate the repulsion at all distances, we must create opposite menisci between the two solids. One simple way to create the opposite menisci is by two microscope slides, one held vertically on water but partially submerged. Glass, being hydrophilic, forms a regular meniscus with water. The other slide is allowed to float on water which forms a reverse meniscus, since glass is heavier than water. When brought close to each other, the plates repel. As another example, we take two small pieces of aluminium foil and make two small circular boats (using for example the cap of a pen as a mould to shape the boats). A small hole is pierced at the bottom of one of the boats by a pen tip. The boats are allowed to float on water, the one with the hole upside down, the other on its bottom. The former forms a reverse meniscus, the latter a regular meniscus, since aluminium is hydrophilic. When they are brought close together they repel each other.

The existence of a stable equilibrium point can be verified by floating two plates such as microscope slides, one heavier (or larger) than the other. The unequal weights

give rise to variations in h_1 and h_2. If the variation is large enough, the plates approach each other to the equilibrium configuration at a finite horizontal distance between them. If the plates are pushed towards each other, they repel each other.

The possibility of the formation of a large cluster can be tested as follows. A regular microscope slide can barely float on water by capillarity and buoyancy. Thus, its size might be close to the critical size. We cut several slides with a diamond cutter, each into three squares, and let many squares float on water. They attract each other and form a cluster of nine squares with a little care (without requiring the water surface to be standing still). Here, the perimeter increased by 50% compared to one slide, but the weight increased by 300%. The inner square remains horizontal, whereas the outer ones are tilted forming a square boat.

In the following, we evaluate the energy associated with the meniscus formed by a single or two interacting plates.

5. Energetics

The energy is contributed by the surface energies of the solid–liquid and liquid–vapour interfaces, and the energy due to the hydrostatic head. We are interested in the part of the energy that varies with the height of the triple line, as well as the gap between the solids. If the plate is thin and the meniscus is formed at the edges of the plate, then the solid–vapour and solid–liquid interface areas change only at the edges as the plate is moved in or out of the liquid surface, or as the plates are moved horizontally with respect to each other. The corresponding change in energy owing to the change of interfacial area at the edges is negligible compared to the change in the hydrostatic or the liquid–vapour interface energies. We will thus evaluate the hydrostatic energy, E_H, and the surface energy, E_S, contributed by the liquid–vapour interface only. Furthermore, the change in energy from the reference configuration where the meniscus height is zero is of interest. Thus, in what follows, E_H and E_S indicate the changes in energies per unit length of the plates from the reference configurations. If the plates are bent (e.g. figure 4) or thick, then the change in the solid–liquid interface energy may not be negligible depending on the geometry and shape of the edges of the plates, and can be evaluated from the specific geometry. Here, for simplicity, we assume that such a change in the interfacial energy for the bent plates considered later is small compared to E_S and E_H, and hence the analysis, when applied to the bent plates, is restricted to geometries where the solid–liquid interface energy change is small. The bent plates are introduced only to illustrate a bifurcation phenomenon in menisci.

5.1. *Energy for the meniscus formed by a single plate*

Surface energy of the meniscus

Consider a small element of the meniscus (liquid–vapour interface) of length $\mathrm{d}S$ at an angle θ with the vertical (figure 2*c*). Its horizontal projection is $\mathrm{d}X = \mathrm{d}S\sin\theta$. Then the liquid–vapour interface energy of the element before and after formation of the meniscus is $\gamma\mathrm{d}X$ and $\gamma\mathrm{d}S$, respectively. The elementary change in energy, $\mathrm{d}E_S = \gamma(\mathrm{d}S - \mathrm{d}X) = \gamma l_0(1 - \mathrm{d}x/\mathrm{d}s)(\mathrm{d}\theta/\theta')$, and

$$\frac{E_S}{E_0} = 2\int_{\theta_0}^{\pi/2}(1-\sin\theta)\frac{\mathrm{d}\theta}{\theta'} = 2\int_{\pi/4-\theta_0/2}^{0} -2\sin\beta\,\mathrm{d}\beta = 4(1-\cos\beta_0), \qquad (5.1)$$

where $\beta = \frac{1}{4}\pi - \frac{1}{2}\theta$, $\beta_0 = \frac{1}{4}\pi - \frac{1}{2}\theta_0$, $E_0 = l_0\gamma$, the factor 2 outside the integral accounts for the two menisci on either side of the plate, and θ' is defined by (3.6).

Hydrostatic energy of the meniscus

It is contributed by the liquid column under the plate and the column of the liquid under the liquid–vapour interface. The former gives an energy $E_{H1} = \rho g H_0^2 W = \rho g l_0^3 h_0^2 w = E_0 h_0^2 w$ where H_0 is the height of the column under the solids surface, $2W$ is the width of the plate, $w = W/l_0$ and $h_0 = H_0/l_0$. The contribution of the liquid column under the liquid–vapour interface can be evaluated by considering a small segment of the interface $\mathrm{d}S$ with column height $H(S)$. The energy due to the elementary column is $\mathrm{d}E_{H2} = \frac{1}{2}\rho g H(S)^2 \mathrm{d}X$, where $\mathrm{d}X$ is the horizontal projection of $\mathrm{d}S$ (figure 2*c*). From (3.3), $\gamma(\mathrm{d}\theta/\mathrm{d}S) = \rho g H(S)$ giving $H(S) = l_0^2(\mathrm{d}\theta/\mathrm{d}S) = l_0^2(\mathrm{d}\theta/l_0\mathrm{d}s) = l_0\theta'$. Thus,

$$E_{H2} = 2\rho g \int_0^\infty \tfrac{1}{2} H^2 \,\mathrm{d}X = \rho g \int_{\theta_0}^{\pi/2} l_0^3 \theta' \sin\theta \mathrm{d}\theta = 2E_0[-\tfrac{2}{3} + \cos\beta_0 - \tfrac{1}{3}\cos(3\beta_0)], \quad (5.2)$$

where the upper limit $\theta = \frac{1}{2}\pi$ is arrived at as $s \to \infty$. Note that E_{H2} accounts for the hydrostatic energy of the meniscus on both sides of the plate. The total energy, $E = E_S + E_{H1} + E_{H2}$, normalized by E_0, is given by

$$\frac{E}{E_0} = \tfrac{8}{3} + wh_0^2 - 2\cos\beta_0 - \tfrac{2}{3}\cos(3\beta_0). \quad (5.3)$$

Note that $E = 0$ when $\theta_0 = \frac{1}{2}\pi$ and $H_0 = 0$, i.e. when the meniscus is horizontal. Since $H_0 = 2l_0 \sin\beta_0$ (equation (3.5)), energy of the meniscus can also be expressed in terms of H_0 or $h_0 = H_0/l_0$:

$$\frac{E}{E_0} = \tfrac{8}{3} + wh_0^2 - \sqrt{1 - \tfrac{1}{4}h_0^2}\,(\tfrac{8}{3} - \tfrac{2}{3}h_0^2), \quad (5.4)$$

which, for small h_0, has a quadratic form:

$$\frac{E}{E_0} = (1 + w)h_0^2, \quad (5.5)$$

i.e. capillarity and buoyancy together behave as a 'linear spring' with a spring constant $2\gamma(1 + w)/l_0$ (unit: force/unit length of the plate/unit displacement) against displacement $l_0 h_0$. Note that here the plate thickness t is small and $t/l_0 \ll h_0 \ll 1$. A typical plate thickness in micro mechanical systems is on the order of 1–5 μm (say 0.002 mm). If the meniscus is between water and air, then $l_0 = 2.72$ mm and $t/l_0 = 0.0007$.

5.2. *Energy barrier for sinking*

The energy necessary to wet a thin flat plate already interfacing with a liquid with its bottom surface is $E_{wet} = 2W(\gamma + \gamma_{sl} - \gamma_s)$ per unit length of the plate. Then, by (2.1), $E_{wet} = 2E_0 w(1 - \cos\phi)$. Now, the total energy, E, of the meniscus as the height of the triple point changes from $H_0 = 0$ is $E = E_S + E_{H1} + E_{H2}$, which can be expressed as a function of θ_0 or H_0. When the plate is moved towards the liquid, then $\theta_0 > \frac{1}{2}\pi$. At the impending collapse of the meniscus, $\theta_0 = \frac{1}{2}\pi + \phi$, and $E_{H1}/E_0 = wh_0^2 = 2w(1 - \cos\phi) = E_{wet}/E_0$ (equation (3.4)). Thus, the energy barrier for sinking, $E_b = E(\theta_0 = \frac{1}{2}\pi + \phi) - E_{wet} = E_S + E_{H2}$ at $\theta_0 = \frac{1}{2}\pi + \phi$. From (5.1) and (5.2), E_b increases monotonically from zero with $0 \leqslant \phi \leqslant \pi$. Thus, E_b is less for a hydrophilic plate ($\phi < \frac{1}{2}\pi$) than that for a hydrophobic plate ($\phi > \frac{1}{2}\pi$).

5.3. *Energy for the menisci formed by two plates*

Here, the total energy, E, is contributed by the two outer menisci (designated by the subscripts L and R for left- and right-hand sides) and the meniscus between the two

plates, each meniscus contributing two components, the hydrostatic and the surface tension parts. The procedure of evaluating them is essentially the same as described for the single plate.

Two plates with a meniscus containing $\mathrm{d}\theta/\mathrm{d}s = 0$

Let the surface and hydrostatic energies of the outer menisci be E_{Sj} and E_{Hj}, $j = L, R$, respectively. Then, E_{Sj} and E_{Hj} are given by (5.1) and (5.2) where $\beta_j = \frac{1}{4}\pi - \frac{1}{2}\theta_j$ replaces β_0. θ_L and θ_R are shown in figure 6(a) and can be obtained from (3.5) for given h_j where θ_0 is replaced by θ_j. The surface energy, E_{S12}, for the meniscus $\mathscr{L}_1\mathscr{L}_2$ is given by

$$\frac{E_{S12}}{E_0} = \int_{\theta_0}^{\theta_1} (1 - \sin\theta)\frac{\mathrm{d}\theta}{\theta'} + \int_{\theta_0}^{\theta_2} (1 - \sin\theta)\frac{\mathrm{d}\theta}{\theta'}, \tag{5.6}$$

where θ' is defined in (4.2). For given heights of $\mathscr{L}_1$ and $\mathscr{L}_2$, and the distance x_0 between the plates, θ_0, θ_1 and θ_2 are obtained by the procedure outlined in § 4.1.

Following § 5.1, the total hydrostatic energy, E_H, can be obtained from

$$E_H = E_0(w_1 h_1^2 + w_2 h_2^2) + E_{HL} + E_{HR} + E_{H12}, \tag{5.7}$$

where $2w_i$, $i = 1, 2$ is the non-dimensional width of the plates, E_{Hj}, $j = L, R$, can be obtained from (5.2) where β_0 is replaced by β_j, and

$$\frac{E_{H12}}{E_0} = \frac{1}{2}\sum_{i=1}^{2} \int_{\theta_0}^{\theta_i} \theta' \sin\theta \mathrm{d}\theta.$$

The total energy is then given by

$$E = E_{SL} + E_{SR} + E_{S12} + E_H. \tag{5.8}$$

Two plates with a meniscus containing $\theta \neq \frac{1}{2}\pi$

Here, the total energy is defined as in (5.8), where E_{SL} and E_{SR} are given by (5.1) with β_j, $j = L, R$ replacing β_0 (figure 6b), E_{Hj} is given by (5.2), and

$$\frac{E_{S12}}{E_0} = \int_{\theta_1}^{\theta_2} (1 - \sin\theta)\frac{\mathrm{d}\theta}{\theta'}, \quad \frac{E_{H12}}{E_0} = \frac{1}{2}\int_{\theta_1}^{\theta_2} \theta' \sin\theta \mathrm{d}\theta, \tag{5.9}$$

where θ' of (5.9) is given by (4.8). Figure 9(e) shows the total energy of the menisci formed by the two plates of figure 9 as a function of the gap, x_0, between the plates. Here, $w_1 = w_2 = 1$ is used for the plates, the energy is normalized by E_0 and the distances by l_0. A numerical derivative of E/E_0 with respect to x_0 is carried out using a linear interpolation between the energy values. The derivative coincides with the force displacement relation (figure 9d).

6. Bifurcation solutions for the meniscus between two solids

It was shown in § 3.3 that for a prescribed height, there are at most two possible menisci between the edge of a single plate and a liquid. Thus, for the meniscus between two plates (two edges are involved) there are at most four possible menisci for given prescribed heights of the triple points. However, the four solutions will result in four different horizontal gaps, x_0, between the plates.

Figures 10(a)–10(d) show the four possible menisci formed between two solids, S_1 with $h_1 = 1.5$ and S_2 with $h_2 = -1$. The angle of the menisci at $\mathscr{L}_1$ with the vertical,

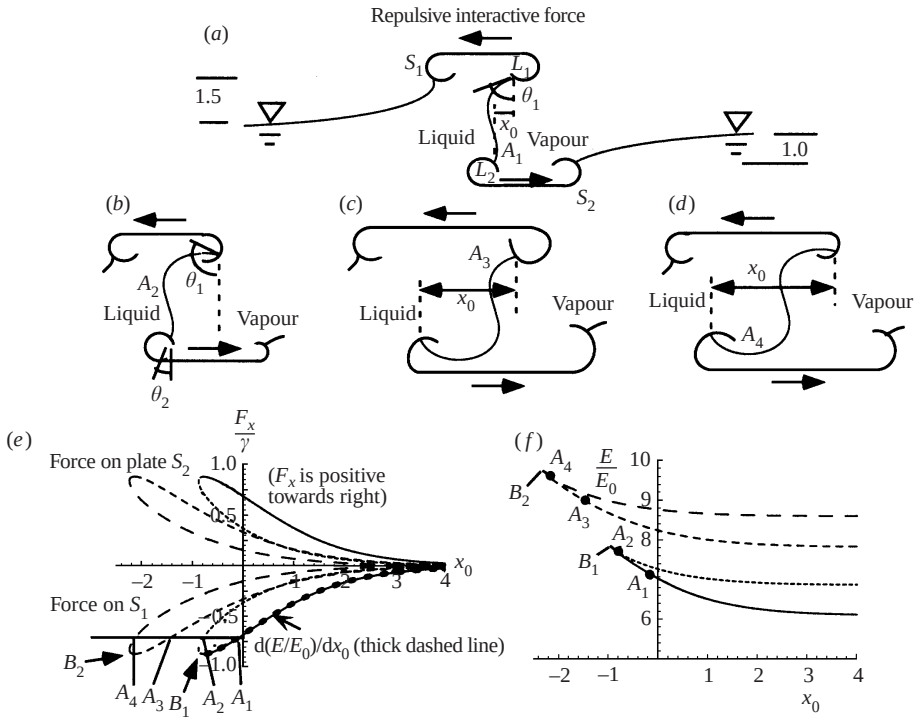

FIGURE 10. Four computed menisci (§4.1), A_1–A_4, between two curved plates, S_1 and S_2, for given normalized heights $h_1 = 1.5$ and $h_2 = -1.0$ of the triple points are shown. The plates are curved such that, at the triple (solid–liquid–vapour) points, the angle of the menisci with the vertical can take appropriate values necessary to form four different menisci, and yet satisfy the fixed contact angle with the solid. The outer menisci are computed by the procedure outlined in §3.4. The interaction force between S_1 and S_2 (in (e)) is repulsive at all non-dimensional distance, x_0, between the triple points. There are four solutions for the force originating from two bifurcation points B_1 and B_2. The points A_1–A_4 correspond to the menisci shown in (a)–(d). The energy (hydrostatic and surface) as a function of x_0 is shown in (f). A numerical derivative of the lowest energy with respect to x_0 coincides with the corresponding force–distance curve of (e) as expected.

θ_1, is close to $-\frac{1}{2}\pi$ (in figure 10(a), $\theta_1 > -\frac{1}{2}\pi$, in 10($b$), $\theta_1 < -\frac{1}{2}\pi$). Thus, the menisci are close to the bifurcation point $\theta_1 = -\frac{1}{2}\pi$. Note that the solids are curved at the edges so that they allow θ_1 and θ_2 to take required values to sustain the menisci $\mathscr{L}_1\mathscr{L}_2$ that maintain the fixed contact angle ϕ between the solid and the liquid. Figure 10(e) shows the four bifurcation branches of the solution for the repulsive interaction force between the two solids as a function of the horizontal gap, x_0 (non-dimensional), between $\mathscr{L}_1$ and $\mathscr{L}_2$. The equal interaction force for the menisci $A_1 - A_4$ are shown by the ordinate of the line A_1A_4 in figure 10(e). Each pair of menisci, such as A_1 and A_2, originate from a bifurcation point such as B_1 where $\theta_1 = -\frac{1}{2}\pi$. The pair, A_3 and A_4, originate from B_2 where $\theta_2 = -\frac{1}{2}\pi$. Figure 10($f$) shows the energy associated with the four possible menisci as a function of x_0. In calculating the hydrostatic part of the energy, the width of each of the plates in non-dimensional units is taken as $2w = 2$. The energies corresponding to the four menisci A_1–A_4 are represented by the filled circles A_1–A_4 in figure 10(f). The lowest energy curve is differentiated with respect to x_0 numerically and the result is plotted on the force diagram. It matches the corresponding force curve as expected.

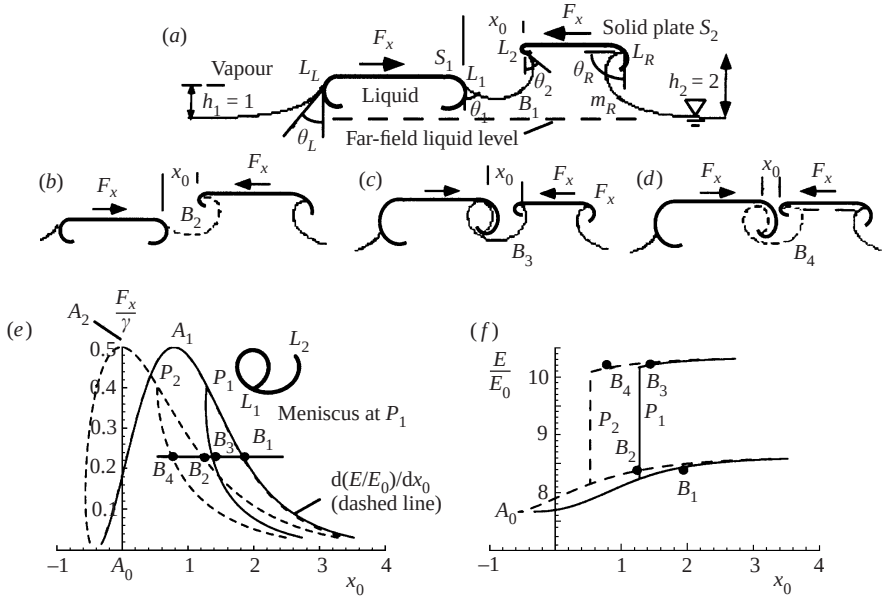

FIGURE 11. (*a–d*) Four possible menisci between two plates S_1 and S_2 with non-dimensional heights 1 and 2. The interaction force is identical for these four menisci. The plates are curved such that at the triple (solid–liquid–vapour) point the angle of the meniscus with the vertical can take the appropriate values resulting in four different menisci, and yet the meniscus can satisfy the fixed contact angle with the solid. The interaction force between S_1 and S_2 as a function of x_0 is shown in (*e*) where the points B_1–B_4 correspond to the menisci B_1–B_4 of (*a*)–(*d*). The four solutions B_1–B_4 originate from two bifurcation points P_1 and P_2. The meniscus, $\mathscr{L}_1\mathscr{L}_2$, between the solids at P_1 is also shown. The energy (hydrostatic and surface) as a function of x_0 is shown in (*f*). A numerical derivative of the lowest energy with respect to x_0 coincides with the corresponding force–distance curve as expected.

Figures 11(*a*)–11(*d*) show the four possible menisci between two solids S_1 and S_2 with $h_1 = 1$ and $h_2 = 2$, respectively. Note that $h = 2$ is the maximum allowable height (see (3.5) and the following paragraph) of the meniscus m_R on the right-hand side of S_2 with an angle $\theta_R = -\frac{1}{2}\pi$ at the triple point $\mathscr{L}_R$. Figure 11(*e*) shows the interaction force, F_x/γ, which is attractive for all x_0. The force corresponding to the four menisci, B_1–B_4, are shown by filled circles B_1–B_4 in figure 11(*e*). The solutions B_1 and B_3 are two bifurcation branches originating from P_1 where the meniscus becomes closed. For $x_0 < x_{0P_1}$, where x_{0P_1} is the distance between $\mathscr{L}_1$ and $\mathscr{L}_2$ at state P_1, the meniscus of type B_3 becomes non-physical, since it intersects with itself and continues beyond the point of intersection. Hence, only the meniscus of type B_1 is retained. The solutions B_2 and B_4 originate from P_2, and at $x_0 < x_{0P_2}$ the meniscus of type B_4 becomes non-physical, and the solution of type B_2 is retained. The interaction force reaches equal maximum at A_1 and A_2. Here, $\theta_1 = \frac{1}{2}\pi$ and hence the capillary force on S_1 acts towards the right, and reaches its maximum value $\gamma(\sin(\frac{1}{2}\pi) - \sin\theta_L)$. For the solid S_2, the tangent to the meniscus at $\mathscr{L}_2$ deviates most from $\theta_2 = \frac{1}{2}\pi$, and the force towards the left maximizes with the value $\gamma(\sin(\frac{1}{2}\pi) - \sin\theta_2)$, and is equal to the force on S_1 towards the right. The menisci A_1 and A_2 originate from A_0 where the interaction force vanishes, and $x_0 < 0$. Here, $\theta_2 = \frac{1}{2}\pi$, and hence the capillary force on both edges of S_2 cancel each other. Note that, $\theta_2 = \frac{1}{2}\pi$ is also the required initial angle for a single meniscus with $h = 2$. The angle of this meniscus with the vertical

when it reaches a height $h = 1$ must be the same as the initial angle for a single meniscus with $h = 1$, such as that formed by S_1 on its left-hand side with an angle θ_L satisfying (3.5) for $h = 1$. However, $\pi - \theta_L$ also satisfies (3.5) which is the value taken by θ_1 at $\mathscr{L}_1$, i.e. $\theta_1 = \pi - \theta_L$. At A_0, $\theta_1 = \pi - \theta_L$ and hence the net horizontal force on S_1 is $\gamma(\sin\theta_L - \sin(\pi - \theta_L)) = 0$. No solution for the meniscus exists for $x_0 < x_{0A_0}$. The energy variations for the menisci as a function of x_0 are shown in figure 11(f) where $w = 1$ is chosen for both the solids. Here, B_1–B_4 correspond to the menisci B_1–B_4 in figure 11(a)–11(d). The points P_1 and P_2 in the force diagram become jumps in the energy diagram owing to the higher energy associated with the loop in the meniscus of types B_3 and B_4. The lowest energy curve (non-dimensional) is differentiated with respect to x_0 numerically using a linear interpolation between adjacent energy values, and the derivative is plotted on the force diagram. As expected, the derivative coincides with the corresponding force–distance curve.

7. Conclusions

The study is motivated by the recent micro fluidic applications where thin plates may form menisci with a liquid and mutually interact with one another. In order to determine the meniscus, we assume that the solid–liquid contact angle and the interfacial energies are fixed. Thus, as a plate forming a meniscus is moved in or out of the liquid, the meniscus is allowed to take its necessary profile by changing its initial angle and yet maintain the fixed contact angle at the edge of the plate. Hence, the range of menisci that can be formed as the plate is moved depends on the geometry of the edge, e.g. the range is larger for a circular edge than a semicircular one. The profile of the meniscus is solved for a one-dimensional case, i.e. for a long plate using the Young–Laplace equation. The height of the triple point, and hence of the plate if it is thin, from the far-field liquid surface is prescribed.

The study is then extended to investigate the interaction between two long plates forming menisci with shallow to steep slopes using the Young–Laplace equation without linearization. Here, the heights of the triple points, and hence of the plates if they are thin, are prescribed, in contrast to earlier interaction studies where the long solids are floating and their heights are determined by their weights. It is found that (i) the interaction force is attractive for two identical menisci, (ii) the interaction force is repulsive for opposite menisci, e.g. one plate is raised and the other plate is depressed below the liquid surface, (iii) for similar menisci but not identical, e.g. one plate is raised more than the other, the force is attractive at long distances, and depending on the menisci heights, the force may be repulsive at short distances with a stable equilibrium in between, (iv) for given heights of the menisci, there can be at most four possible profiles of the meniscus between the plates. The interaction force between two plates is completely determined by the menisci they form. Hydrophilicity or hydrophobicity are parameters that play a role in defining the geometry of the meniscus through the contact angle ϕ, but other parameters such as heights of plates and the geometry of their edges also play a role. Thus, there may be attraction between two hydrophobic plates or two hydrophilic plates, or between a hydrophobic and a hydrophilic plate depending on the menisci they form.

Two universal bounds are established for menisci in a space non-dimensionalized by the capillary length l_0. They are applicable to thick or thin solids, as long as the solids form one-dimensional menisci with the liquid, i.e. one of the principal curvatures of the menisci vanishes. The bounds are: for a meniscus between two solids at a finite distance apart, (i) if there is a point on the meniscus where the curvature vanishes

(and hence the height vanishes) then the absolute heights of the triple points can be at most 2, but (ii) if there is a point P on the meniscus where the tangent is horizontal with liquid below, and where the height is h_0, then $|h_0| > 0$, the heights h_1 and h_2 of the triple points are of same sign as that of h_0, and $4 \geqslant h_i^2 - h_0^2 \geqslant 0$, $i = 1, 2$. The two families of menisci, (i) and (ii), are mutually exclusive. Also, the height of a meniscus with a single solid can be at most 2 above or below the liquid surface.

The work was supported by NSF CAREER Award (NSF ECS 97-34368). Special thanks to Professor Ronald Adrian, University of Illinois at Urbana-Champaign (UIUC), for the many illuminating discussions I had with him on this topic. Thanks to Professor Hassan Aref for introducing me to some of the key references in the field. I am indebted to Professor Arne Pearlstein of UIUC who thoroughly edited the manuscript with great patience. Thanks to Professors Leslie Phinney and Ed Damiano of UIUC for their valuable comments and encouragement in completing the manuscript. Finally, I am grateful to the referees of the manuscript as well as to Professor Howard Stone for their time and effort, and for the pleasure I derived in addressing their questions. They have contributed to strengthening the paper. Science can only progress and understanding deepen through a thorough critique of our works by sharp minds.

REFERENCES

Allain, C. & Cloitre, M. 1988 Horizontal cylinders at a fluid interface: equilibrium, shape of the meniscus and capillary interaction. *Ann. Physique* **13**, 141–146.

Batchelor, G. K. 1967 *An Introduction to Fluid Dynamics*, p. 67. Cambridge University Press.

Bowden, N., Arias, F., Deng, T. & Whitesides, G. M. 2001*a* Self-assembly of microscale objects at a liquid/liquid interface through lateral capillary forces. *Langmuir* **17**, 1757–1765.

Bowden, N., Choi, I. S., Grzybowski, B. A. & Whitesides, G. M. 1999 Mesoscale self-assembly of hexagonal plates using lateral capillary forces: synthesis using the 'capillary bond'. *J. Am. Chem. Soc.* **121**, 5373–5391.

Bowden, N., Oliver, S. R. J. & Whitesides, G. M. 2000 Mesoscale self-assembly: capillary bonds and negative menisci. *J. Phys. Chem.* B **104**, 2714–2724.

Bowden, N., Terfort, A., Carbeck, J. & Whitesides, G. M. 1997 Self-assembly of mesoscale objects into ordered two-dimensional arrays. *Science* **276**, 233–235.

Bowden, N. B., Weck, M., Choi, I. S. & Whitesides, G. M. 2001*b* Molecule-mimetic chemistry and mesoscale self-assembly. *Accts Chem. Res.* **34**, 231–238.

Bragg, W. L. & Nye, J. F. 1947 A dynamical model of a crystal structure. *Proc. R. Soc. Lond.* A **190**, 474–481.

Bustillo, J. M., Howe, R. T. & Muller, R. S. 1998 Surface micromachining for microelectromechanical systems. *Proc. IEEE* **86**, 1552–1574.

Carey, V. P. 1992 *Liquid–Vapor Phase-Change Phenomena*, pp. 38, 76. Hemisphere.

Chan, D. Y. C., Henry, Jr, J. D. & White, L. R. 1981 The interaction of colloidal particles collected at fluid interfaces. *J. Colloid Interface Sci.* **79**, 410–418.

Choi, I. S., Bowden, N. & Whitesides, G. M. 1999 Shape-selective recognition and self-assembly of mm-scale components. *J. Am. Chem. Soc.* **121**, 1754–1755.

Concus, P. 1968 Static menisci in a vertical right circular cylinder. *J. Fluid Mech.* **34**, 481–495.

de Gennes, P. G. 1985 Wetting: statics and dynamics. *Rev. Mod. Phys.* **57**, 827–863.

Gibbs, J. W. 1906 *The Scientific Papers of J. Willard Gibbs, vol. 1, Thermodynamics*. Dover (Dover reprint 1961).

Gifford, W. A. & Scriven, L. E. 1971 On the attraction of floating particles. *Chem. Engng Sci.* **26**, 287–297.

Grzybowski, B. A., Bowden, N., Arias, F., Yang, H. & Whitesides, G. M. 2001 Modeling of menisci and capillary forces from the millimeter to the micrometer size range. *J. Phys. Chem.* B **105**, 404–412.

Grzybowski, B. A., Stone, H. A. & Whitesides, G. M. 2000 Dynamic self-assembly of magnetized, millimeter-sized objects rotating at a liquid–air interface. *Nature* **405**, 1033–1036.

Hildebrand, M. A. & Tallmadge, J. A. 1970 Corrected values for static menisci on the outside of cylinders. *J. Fluid Mech.* **44**, 811–812.

Hosokawa, K., Shimoyama, I. & Miura, H. 1996 Two-dimensional micro-self-assembly using the surface tension of water. *Sensors Actuat.* A **57**, 117–125.

Kim, C.-J. 1999 Micromachines driven by surface tension. *Proc. 30th AIAA Fluid Dyn. Conf. 28 June–1 July, 1999, Norfolk, Virginia, USA*. AIAA 99-3800.

Kladits, P. E. & Bright, V. M. 2000 Novel resistive point heater for mems remote solder self assembly. *Proc. 2000 ASME Intl Mech. Engng Congr. and Expos. Micro-Electro-Mechanical Systems (MEMS) – 2000, Orlando, Florida, 5–10 November*. MEMS vol. 2, pp. 161–167.

Kralchevsky, P. A. & Nagayama, K. 2000 Capillary interactions between particles bound to interfaces, liquid films and biomembranes. *Adv. Colloid Interface Sci.* **85**, 145–192.

Kralchevsky, P. A., Paunov, V. N., Denkov, N. D. & Nagayama, K. 1994 Capillary image forces I. Theory. *J. Colloid Interface Sci.* **167**, 47–65.

Kralchevsky, P. A., Paunov, V. N. & Nagayama, K. 1995 Lateral capillary interaction between particles protruding from a spherical liquid layer. *J. Fluid Mech.* **299**, 105–132.

Kuiper, S., Boer, M. D., Rijn, C. V., Nijdam, W., Krijnen, G. & Elwenspoek, M. 2000 Wet and dry etching techniques for the release of sub-micrometer perforated membranes. *J. Micromech. Microengng* **10**, 171–174.

Laplace, P. S. 1966 First published by Laplace in 1806 *Celestial Mechanics*, vol. IV (translation from French to English by N. Bowditch). Chelsea Publishing, New York.

Liu, R. H., Stremler, M. A., Sharp, K. V., Olsen, M. G., Santiago, J. G., Adrian, R. J., Aref, H. & Beebe, D. J. 2000 Passive mixing in a three dimensional serpentine microchannel. *J. Microelectromech. Syst.* **9**, 190–197.

Majumdar, S. R. & Michael, D. H. 1976 The equilibrium and stability of two dimensional pendent drops. *Proc. R. Soc. Lond.* A *Math. Phys. Sci.* **351**, 89–115.

Mansfield, E. H., Sepangi, H. R. & Eastwood, E. A. 1997 Equilibrium and mutual attraction or repulsion of objects supported by surface tension. *Phil. Trans. R. Soc. Lond.* A *Phys. Sci. Engng* **355**, 869–919.

Manz, A., Miyahara, Y., Miura, J., Watanabe, Y., Miyagi, H. & Sato, K. 1990 Design of an open-tubular column liquid chromatograph using silicon chip technology. *Sensors Actuat.* B *Chemical* **B1**, 249–255.

Maxwell, J. C. 1878 Capillary action. In *Encyclopedia Britannica*, 9th edn, vol. V, p. 67. Charles Scribner.

Nicolson, M. M. 1949 The interaction between floating particles. *Proc. Camb. Phil. Soc.* **45**, 288–295.

Oliver, J. F., Huh, C. & Mason, S. G. 1977 Resistance to spreading of liquids by sharp edges. *J. Colloid Interface Sci.* **59**, 568–581.

Orr, F. M., Scriven, L. E. & Rivas, A. P. 1975 Pendular rings between solids: meniscus properties and capillary force. *J. Fluid Mech.* **67**, 723–742.

Padday, J. F. 1971 The profiles of axially symmetric menisci. *Phil. Trans. R. Soc. Lond.* A **269**, 265–293.

Padday, J. F., Petre, G., Rusu, C. G., Gamero, J. & Wozniak, G. 1997 The shape, stability and breakage of pendant liquid bridges. *J. Fluid Mech.* **352**, 177–204.

Padday, J. F. & Pitt, A. 1971 Axisymmetric meniscus profiles. *J. Colloid Interface Sci.* **38**, 323–334.

Padday, J. F., Pitt, A. R. & Pashley, R. M. 1975 Menisci at a free liquid surface: surface tension from the maximum pull on a rod. *J. Chem. Soc. Faraday Trans.* I **71**, 1919–1931.

Paunov, V. N., Kralchevsky, P. A., Denkov, N. D. & Nagayama, K. 1993 Lateral capillary forces between floating submillimeter particles. *J. Colloid Interface Sci.* **157**, 100–112.

Poisson, S. D. 1831 *Nouvelle Theorie de L'action Capillaire*, p. 226, also see figs. 5, 6, 16, 21. Bachelier, Paris.

Popov, E. P. 1976 *Mechanics of Materials*, 2nd edn. Prentice Hall.

Sager, C. & Saif, T. 1999 Capillary forces at the interface of a mems actuator. *Proc. 1999 ASME Intl Mech. Engng Congr. and Expos. MEMS 99, Nashville, TN, 14–19 November*. MEMS vol. 1, pp. 365–370.

Saif, M. T. A. 2000 A study on the interaction force between two small bodies on a liquid for micro self assembly and separation. *Proc. 2000 ASME Intl Mech. Engng Congr. and Expos. Micro-*

Electro-Mechanical Systems (*MEMS*) *2000, Orlando, Florida, 5–10 November*. MEMS vol. 2, pp. 481–487.

Saif, M. T. A., Alaca, E. & Sehitoglu, H. 1999 Analytical modeling of electrostatic membrane actuator for micro pumps. *J. Microelectromech. Syst*. **8**, 335–345.

Soerensen, O., Drese, K. S., Ehrfeld, W. & Hartmann, H. J. 1999 Micromachined flow handling components: micropumps. *Proc. Spie Intl Soc. Optical Engng* **3857**, 52–60.

Syms, R. R. A. 1999 Surface tension powered self-assembly of 3-D micro-optomechanical structures. *J. Microelectromech. Syst*. **8**, 448–455.

Temmel, G., Hermes, T., Paneva, R., Kluge, S. & Wolas, P. 1996 A micro mechanical system for liquid dosage and nebulization. *Proc. Actuator 96. 5th Intl Conf. New Actuators. 26–28 June 1996, Bremen, Germany, AXON Technologie Consult GmbH*. (ed. H. Borgmann), pp. 57–60.

Terfort, A., Bowden, N. & Whitesides, G. M. 1997 Three-dimensional self-assembly of millimeter-scale components. *Nature* **386**, 162–164.

Velev, O. D., Denkov, N. D., Paunov, V. N., Kralchevsky, P. A. & Nagayama, K. 1994 Capillary image forces II. Experiment. *J. Colloid Interface Sci*. **167**, 66–73.

Vogel, T. I. 1982 Symmetric unbounded liquid bridges. *Pacific J. Maths* **103**, 205–241.

Warren, M. E., Sweatt, W. C., Jr, Bailey, C. G., Matzke, C. M., Arnold, D. W., Kemme, S. A., Allerman, A. A., Carter, T. R., Asbill, R. E. & Samora, S. 1999 Integrated micro-optical fluorescence detection system for microfluidic electrochromatography. *Proc. Spie Intl Soc. Optical Engng* **3878**, 185–192.

White, D. A. & Tallmadge, J. A. 1965 Static menisci on the outside of cylinders. *J. Fluid Mech*. **23**, 325–335.

Young, T. 1805 An essay on the cohesion of fluids. *Phil. Trans. R. Soc. Lond*. **95**, 65–87.